Local Observation of Reverse-Domain Superconductivity in a Superconductor-Ferromagnet Hybrid

J. Fritzsche,[1] V. V. Moshchalkov,[1] H. Eitel,[2] D. Koelle,[2] R. Kleiner,[2] and R. Szymczak[3]

[1]*INPAC - Institute for Nanoscale Physics and Chemistry, Nanoscale Superconductivity and Magnetism & Pulsed Fields Group, Katholieke Universiteit Leuven, Celestijnenlaan 200D, B-3001 Leuven, Belgium*

[2]*Physikalisches Institut—Experimentalphysik II, Universität Tübingen, Auf der Morgenstelle 14, D-72076 Tübingen, Germany*

[3]*Institut of Physics, Polish Academy of Science, al. Lotnikow 32/46, Warszawa 02-668, Poland*

(Received 25 April 2006; published 22 June 2006)

Nanoscale magnetic and superconducting properties of the superconductor-ferromagnet $Nb/PbFe_{12}O_{19}$ hybrid were studied as a function of applied magnetic fields. Low-temperature scanning laser microscopy (LTSLM) together with transport measurements were carried out in order to reveal local variations of superconductivity induced by the magnetic field template produced by the ferromagnetic substrate. Room temperature magnetic force microscopy (MFM) was performed and magnetization curves were taken at room and low temperature to investigate the magnetic properties of the hybrid. Comparative analysis of the LTSLM and the MFM images has convincingly demonstrated the presence of the reverse-domain superconductivity.

DOI: 10.1103/PhysRevLett.96.247003 PACS numbers: 74.78.Na, 74.62.−c, 75.60.Ch

Superconductivity and ferromagnetism can be considered to be antagonistic [1] since electrons with opposite spin form Cooper pairs in superconductors, while spin alignment occurs in ferromagnets. However, there are possibilities for the coexistence of these two phenomena, e.g., in artificial superconductor/ferromagnet (S/F) hybrid systems. These artificial systems exhibit a variety of new physical phenomena [for recent reviews, see [2,3]] such as the reverse-domain superconductivity (RDS) and the domain-wall superconductivity (DWS). The latter term refers to the state of an S/F hybrid where the stray field of the magnetic domains of the F layer suppresses superconductivity in the S layer anywhere else than on top of the domains walls (left part of Fig. 1). When superimposing an external magnetic field $\vec{H}_{\rm ext}$, the total magnetic field is enhanced above domains which are polarized parallel to $\vec{H}_{\rm ext}$ (parallel domains). By contrast, on top of domains polarized in the reverse direction (reverse domains), the total magnetic field is weakened. Thus, superconductivity can nucleate on top of reverse domains which then is referred to as RDS (middle part of Fig. 1). Accordingly, if the upper critical field of the S layer is sufficiently high for superconductivity to exist on top of parallel domains, we call this state the parallel domain superconductivity (PDS) (right part of Fig. 1).

The experimental work aimed at the study of S/F hybrids focuses mostly on integrated response measurements due to simplicity compared to direct, local visualization techniques [4]. For example, the existence of RDS and DWS in S/F-hybrid systems was recently demonstrated by means of transport measurements [5,6]. Further investigation of these phenomena was reported by Gillijns *et al.* who used hybrid $S/F/S$ three-layered structures [7]. But up until now, no direct visualization of neither RDS nor DWS in such systems has been carried out. In this Letter, we present direct imaging results by combining the low-temperature scanning laser microscopy (LTSLM) [8–10] and magnetic force microscopy (MFM) techniques to study an S/F hybrid that consists of a thin Nb bridge on top of a $PbFe_{12}O_{19}$ (magnetoplumbite) single crystal.

The basic idea of our experiment is the following: at temperatures slightly below the critical temperature T_c of Nb a pulsed laser scans over the superconducting bridge, that carries a current $I \simeq I_c$ (critical current). The perturbation by the laser at position $\vec{r}$ (in the plane of the Nb film) leads to the destruction of the superconducting state in the area of the laser spot by local heating. As a result, a global increase of resistance R is detected by measuring the voltage drop over the bridge using lock-in techniques. This voltage is proportional to the local derivative

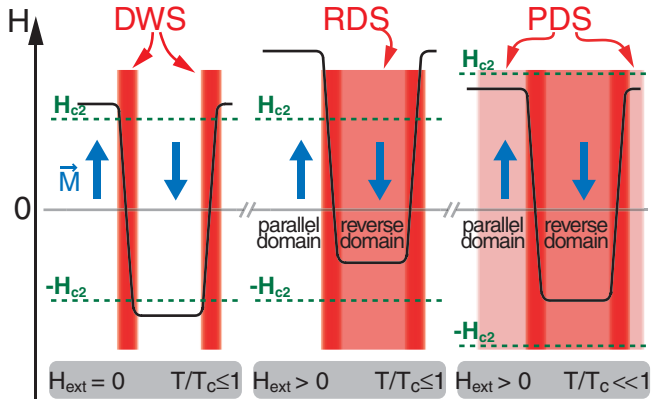

FIG. 1 (color online). Schematic diagram of the total magnetic field H (black line) and the upper critical field H_{c2} in the S layer of an S/F hybrid. Left: superconductivity can only exist within the shaded (red) regions above domain walls (DWS). Middle: additional nucleation of superconductivity above reverse domains due to an external magnetic field (RDS). Right: the entire S layer is superconducting, even on top of parallel domains (PDS).

$dR(\vec{r})/dT$ of the resistance of the bridge [10] with respect to the temperature increase in the laser spot and, therefore, images those areas which are close to $T_c(H)$.

Magnetoplumbite is a well-known ferrimagnet [11,12] with out-of-plane magnetization and domain pattern that depends strongly on magnetic history. We used a $PbFe_{12}O_{19}$ single crystal of approximately 0.6 mm thickness as a substrate on top of which 10 nm Si followed by 30 nm Nb were deposited by molecular beam epitaxy. The reason for separating the superconductor from the ferrimagnet by a buffer layer was to avoid proximity effect. Finally, a bridge-shaped mesa of 40 by 135 μm was carefully etched out of the Nb film using standard electron beam lithography and argon ion milling. In Fig. 2 the room temperature MFM images are presented for different external magnetic fields. Magnetization curves at 296 and 5 K are also given. External fields were produced by underlying permanent magnets and measured at the height of the substrates surface with a Hall probe. The MFM images (Fig. 2) illustrate the magnetic domain patterns of $PbFe_{12}O_{19}$ at different points within the hysteresis loop: close to the remanent state at 25 mT an intertwined maple-leaf-like pattern is formed by the domains, making it rather confusing to figure out their direction of polarization. Contrary to that, already at 74 mT, the reverse domains become thinner and can be distinguished clearly from the parallel domains. The trend of the domain thinning continues at higher fields together with a transition of the reverse domains from chains of spiked rings (127 mT) over isolated branches (151 to 195 mT) to single hollow ovals patterns at 249 mT. The percentage Π of scanning area covered by parallel domains is indicated in Fig. 2 together with normalized magnetization curves of the substrate at high and low temperatures. Apparently, Π mirrors the room temperature magnetization reasonably well. However, it would be premature to conclude that from each value of M the corresponding value of Π can be uniquely defined. The magnetization curves show that the substrate is magnetically extremely soft even though weak hysteresis can be seen close to saturation (see magnified sections of the MH diagram). Moreover, because of the similarity of $M(H)$ at 5 and 296 K, it is reasonable to assume that the behavior of the domains is alike both at room and low temperatures.

In external magnetic fields, the Nb bridge showed two kinds of transition from the superconducting to the normal state, both strikingly different in nature. For each of these kinds, a typical example is shown in the diagram of Fig. 3 where the normalized resistance of the bridge is plotted versus temperature. Mostly, the transitions were characterized by pronounced plateaus similar to the case of 290 mT which is shown here. But sometimes, at low fields, smooth transitions were observed alike the $R(T)$ curve at 200 mT. To clarify the origin of the difference in transition, LTSLM

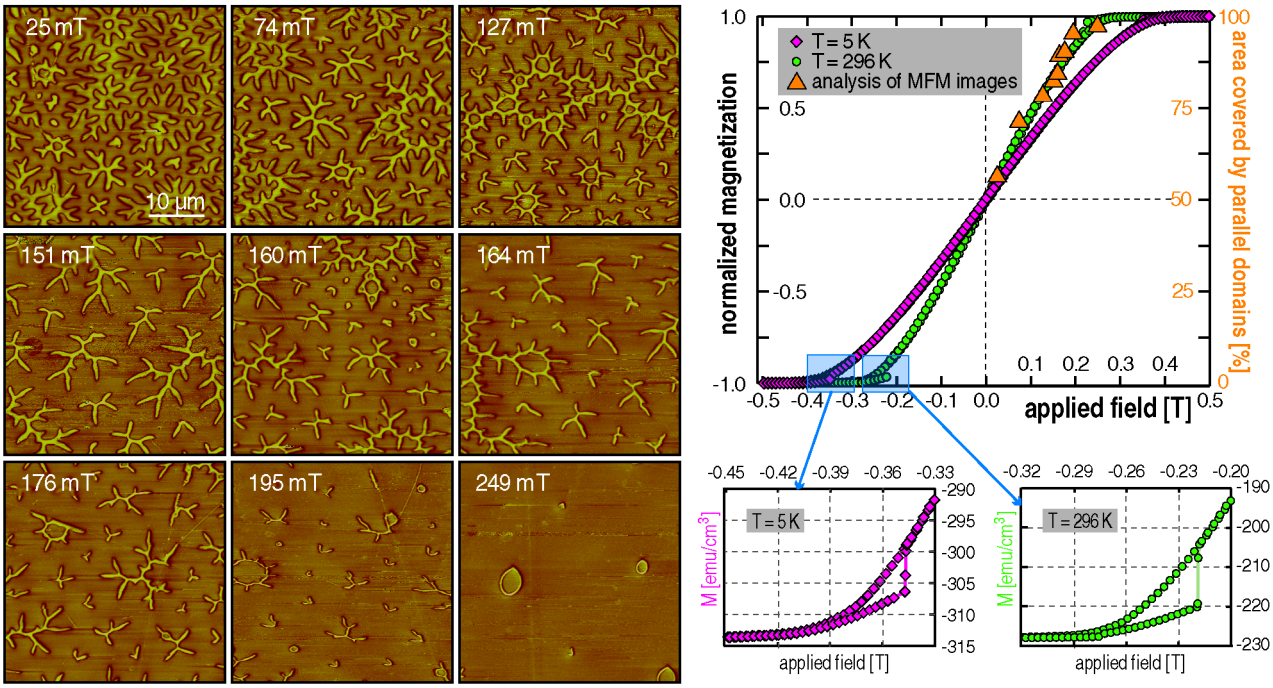

FIG. 2 (color online). Left: room temperature 40×40 μm^2 MFM images of the $PbFe_{12}O_{19}$ substrate in external magnetic fields applied perpendicular to the basal plane. Yellow and brown areas represent domains polarized reverse and parallel to the field, respectively. The separating domain walls are visible as thin dark lines. Right: magnetization curves normalized to saturation values for high and low temperatures. Percentages of the MFM images covered by parallel domains are indicated as orange triangles. Hysteresis effects close to saturation are shown in detail.

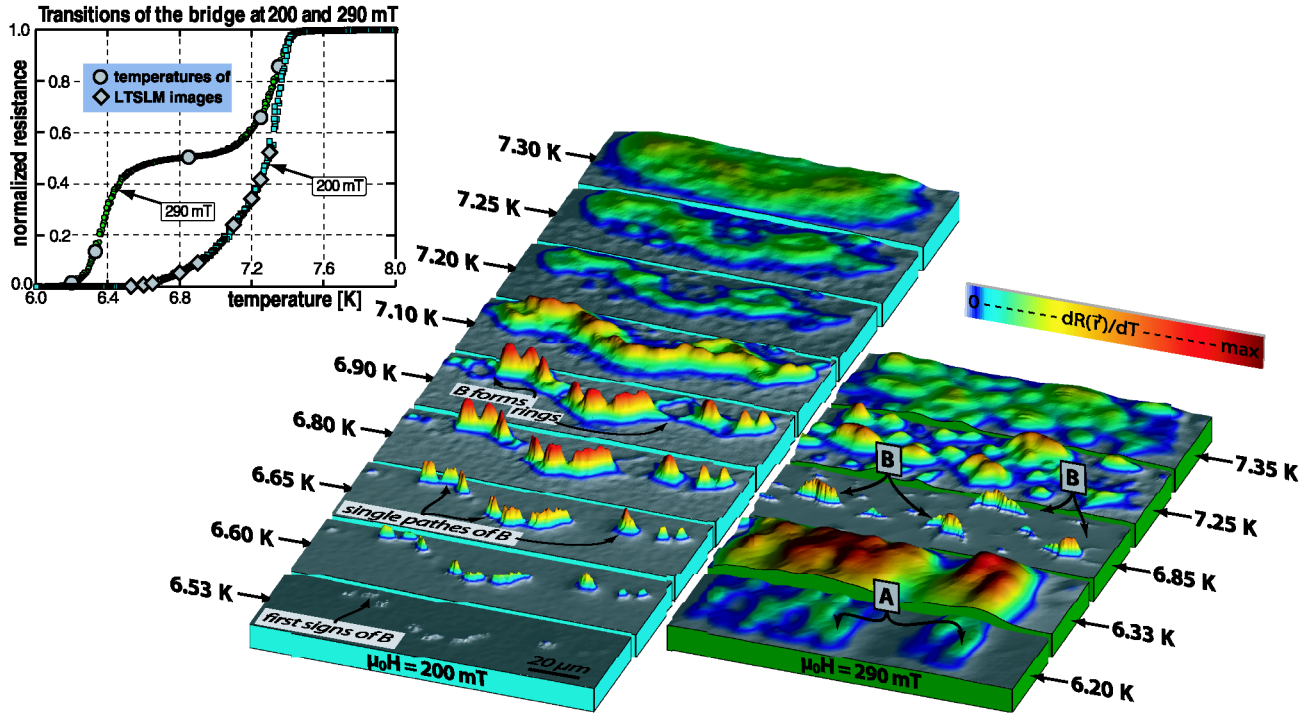

FIG. 3 (color online). Diagram: normalized resistance of the bridge vs temperature at 200 mT and 290 mT. Gray circles and diamonds indicate the temperatures at which the LTSLM images were taken. Images: temperature dependence of the LTSLM $dR(\vec{r})/dT$ signal of the Nb bridge at 200 mT (left series) and 290 mT (right series).

images were taken at those temperatures marked in the diagram of Fig. 3 with gray circles and diamonds.

Let us turn first to the case of 200 mT. From the corresponding LTSLM images which are shown in Fig. 3 (left series), several observations can be made. To begin with, the signal is dominated by a feature B that develops continuously with increasing temperature. At 6.53 K, first signs of B appeared which became clearer when T was raised. All details of B were visible at 6.90 K whereas at higher temperatures, the feature became less defined in shape (7.10 K), weakened (7.20 K), smeared out (7.25 to 7.30 K), and finally faded away. This continuous development is in agreement with the smooth increase of the corresponding resistance, see the $R(T)$ curve in the diagram of Fig. 3. Second, the feature B is extended along the whole bridge and is mostly a single path. But at some places it branches out and forms rings as can be seen in the picture corresponding to 6.90 K. Third, the normalized magnetization of the substrate is the same at 200 mT and 5 K and at 130 mT and 296 K (see Fig. 2). Therefore, at 200 mT and 5 K, a magnetic domain pattern is expected that is similar to that one of the room temperature MFM image taken at 127 mT (Fig. 2). In that case, an extended reverse domain exists that forms a chain of spiked rings. The size of these rings is comparable to the size of the rings formed by B. It is obvious to conclude from these observations that an extended reverse domain connects the left and right side of the bridge, causing an uninterrupted path of RDS in the Nb film. However, only main features of that reverse domain are mirrored in the LTSLM image of the RDS, as those parts of the RDS which did not contribute to current transport could not be detected.

In addition, several details can also be seen in the LTSLM images and well explained with our interpretation. One example is the appearance of small dots next to B at temperatures higher than 6.90 K. In this temperature range, not all the current flows inside the extended path of RDS because the critical current density j_c is too low. Instead, areas of RDS next to B, which are induced by small isolated reverse domains (see Fig. 2 the MFM image at 127 mT), also contribute to the current transport and can therefore be detected. Another example is the difference in temperatures at which rings and single paths of B appear in the LTSLM signal (6.90 and 6.60 K, respectively). Since each ring provides two parallel superconducting paths, heating one branch of the ring causes the current to redistribute to the other branch. As a result, the signals obtained from rings are smaller than those from single paths of B. However, this is only true as long as current redistribution is possible, i.e., as long as j_c is not reached in the rings. Accordingly, at higher temperatures ($T > 6.90$ K), rings and single paths of B are of the same height in the LTSLM signal.

Let us now switch over to the case of 290 mT. Apparently, the LTSLM signal (right series of images in

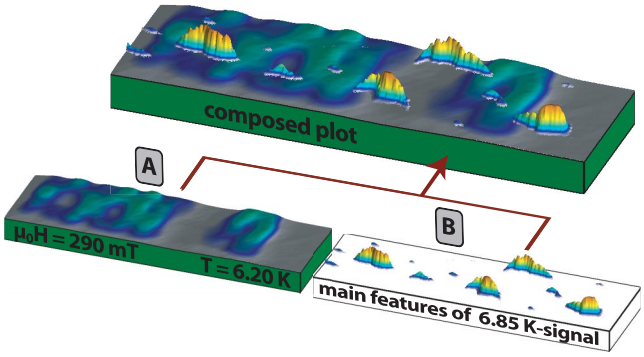

FIG. 4 (color online). Composed plot of the two LTSLM signals, which were obtained in the 290 mT case at 6.20 K (signal *A*) and 6.85 K (signal *B*).

Fig. 3) develops strikingly different in temperature, compared to the LTSLM signal of the just discussed case of 200 mT: at low temperatures (6.20 and 6.33 K), a broad signal *A* was observed which was not very well defined in shape. At 6.85 K, *A* vanished completely and instead, a new signal *B* with small sharp features was detected. This abrupt change in the LTSLM signal goes along with the appearance of the plateau in the corresponding $R(T)$ curve in the diagram of Fig. 3. While at temperatures below the plateau region the signal *A* was seen, in the plateau region and at higher temperatures the signal *B* was observed. In order to compare these two signals, we plotted them on top of each other as illustrated in Fig. 4. This composed picture shows clearly that *A* and *B* are complementary in nature, because in the vicinity of each part of *B*, *A* tends to vanish. Again, interpretation of this observation is possible when taking the MFM images of Fig. 2 into account. At 290 mT and low temperatures, the appearance of elongated reverse domains is to be expected. This suggests that *B* is an image of the RDS while *A* originates from parallel domain superconductivity (PDS). Accordingly, the PDS signal was obtained at a lower temperature than the RDS signal, as T_c on top of parallel domains must be lower than above reverse domains. The PDS signals at 6.20 K do not appear in areas that are ''shorted'' by strongly superconducting paths along the RDS regions showing up as signal *B* at 6.85 K. The same explanation holds for the absence of any PDS signal in the case of 200 mT, where the whole bridge was shorted by one strongly superconducting path of RDS.

In conclusion, we directly visualized the reverse-domain superconductivity (RDS) and the parallel domain superconductivity (PDS) in an artificial $Nb/PeFe_{12}O_{19}$ hybrid system. To do so, we investigated the superconducting and magnetic properties of the hybrid by low-temperature scanning laser microscopy (LTSLM) and magnetic force microscopy (MFM), respectively. Transport measurements were also carried out and suggested the existence of two characteristic states of the *S* layer, dependent on the applied magnetic field and the specific magnetic domain pattern in the *F* layer. These two states are clearly found again in the LTSLM signals, and a straightforward interpretation can be given by taking the MFM images into account: at low external magnetic fields, extended paths of RDS are induced in the *S* layer by continuous reverse domains in the *F* layer, whereas at higher fields, only small isolated regions of RDS survive above the remaining reverse domains.

The authors are thankful to B. Opperdoes for help with sample preparation. This work was supported by the ESF Pi-shift programme, the K. U. Leuven Research Fund GOA/2004/2 program, the Belgian IUAP, and by the Fund for Scientific Research—Flanders (Belgium) (F. W. O.-Vlaanderen).

[1] L. P. Gorkov, Sov. Phys. JETP **9**, 1364 (1959).
[2] I. F. Lyuksytov and V. L. Pokrovsky, Adv. Phys. **54**, 67 (2005).
[3] A. I. Buzdin, Rev. Mod. Phys. **77**, 935 (2005).
[4] L. Crétinon, A. K. Gupta, H. Sellier, F. Lefloch, M. Fauré, A. Buzdin, and H. Courtois, Phys. Rev. B **72**, 024511 (2005).
[5] Z. Yang, M. Lange, A. Volodin, R. Szymczak, and V. V. Moshchalkov, Nat. Mater. **3**, 793 (2004).
[6] A. Yu. Rusanov, M. Hesselberth, J. Aarts, and A. I. Buzdin, Phys. Rev. Lett. **93**, 057002 (2004).
[7] W. Gillijns, A. Yu. Aladyshkin, M. Lange, M. J. Van Bael, and V. V. Moshchalkov, Phys. Rev. Lett. **95**, 227003 (2005).
[8] A. G. Sivakov, A. P. Zhuravel, O. G. Turutanov, and I. M. Dmitrenko, Appl. Surf. Sci. **106**, 390 (1996).
[9] A. G. Sivakov, A. V. Lukashenko, D. Abraimov, P. Müller, A. V. Ustinov, and M. Leghissa, Appl. Phys. Lett. **76**, 2597 (2000).
[10] M. Wagenknecht, H. Eitel, T. Nachtrab, J. B. Philipp, R. Gross, R. Kleiner, and D. Koelle, Phys. Rev. Lett. **96**, 047203 (2006).
[11] P. J. Grundy, Br. J. Appl. Phys. **16**, 409 (1965).
[12] M. W. Muller, Phys. Rev. **162**, 423 (1967).